Computational rheology: challenges and developments

A.M. Afonso[1], F.T. Pinho[2] and M.A. Alves[1]

[1] Centro de Estudos de Fenómenos de Transporte, Departamento de Engenharia Química, Faculdade de Engenharia da Universidade do Porto, Rua Dr. Roberto Frias s/n, 4200-465, Porto, Portugal.

[2] Centro de Estudos de Fenómenos de Transporte, Departamento de Engenharia Mecânica, Faculdade de Engenharia da Universidade do Porto, Rua Dr. Roberto Frias s/n, 4200-465, Porto, Portugal.

Introduction

Computational rheology (CR, defined as numerical methods applied to flows of complex fluids, rather than computational rheometry) is a fairly recent scientific branch of the more generic and broader Computational Fluid Dynamics (CFD). It faces demanding challenges, such as the High Weissenberg Number Problem (HWNP), consisting on the loss of convergence at very low levels of elasticity, quantified by the Weissenberg number (*Wi*). This numerical failure at a moderately low Weissenberg number (*Wi*≈1), is accompanied by numerical inaccuracies and lack of mesh-convergent solutions, particularly when geometrical singularities such as corners or stagnation points are present, due to the exponential growth of the normal stresses at such locations. These singularities are frequent among the benchmark flows that have been set-up to help the development and assessment of the behaviour of the numerical techniques in CR, and which have been studied independently by several research groups, in order to obtain consistently highly accurate numerical solutions. From the proposed CR benchmark flows over the past years, it is now possible to conclude that the favourite geometries are the flow around a cylinder and the 4:1 contraction flow [1]. Several plausible explanations for the HWNP have been identified along the past decades. However, and despite some recent progress, there is not yet a full understanding of its origin and possible solution. Recent developments on the tensorial reformulation of the complex fluids constitutive equations, such as the log-conformation [2], the square-root-conformation [3] or the more generic kernel-conformation [4], allowed further insights into possible solutions or, at least, alleviation of the HWNP. In this work, we present recent results obtained with these new matrix transformation frameworks [2]. For this purpose, this work presents an extensive study on the viscoelastic flow around a confined cylinder in a planar channel flow [5] and the fluid flow in a 4:1 planar contraction [6].

Governing equations and numerical method

To simulate steady incompressible flow of viscoelastic fluids, the mass conservation

$$\nabla \cdot \mathbf{u} = 0\,, \tag{1}$$

and the momentum equation,

$$\rho \frac{\mathrm{D}\mathbf{u}}{\mathrm{D}t} = -\nabla p + \beta \eta_o \nabla^2 \mathbf{u} + \frac{\eta_o}{\lambda}(1-\beta)\nabla \cdot \mathbf{A} \tag{2}$$

need to be solved, together with an evolution equation for the conformation tensor, **A**, here for the Oldroyd-B fluids and based on the log-conformation formulation ($\boldsymbol{\Theta} = \log \mathbf{A}$):

$$\frac{\partial \boldsymbol{\Theta}}{\partial t} + (\mathbf{u}\cdot\nabla)\boldsymbol{\Theta} - (\mathbf{R}\boldsymbol{\Theta} - \boldsymbol{\Theta}\mathbf{R}) - 2\mathbf{E} = \frac{1}{\lambda}\left(e^{-\boldsymbol{\Theta}} - \mathbf{I}\right) \tag{3}$$

The fluid total extra-stress is the sum of solvent and polymer stress contributions. The viscosity ratio, β, is defined as the ratio between the Newtonian solvent viscosity, η_s, and the total zero shear-rate viscosity, η_0, $\beta = \eta_s/\eta_0 = \eta_s/(\eta_s+\eta_P)$ where η_P is the coefficient of viscosity of the polymer.

A fully-implicit finite-volume method (FVM) was used to solve Equations (1)–(3), which is based on a time marching pressure-correction algorithm and is formulated with the collocated variable arrangement [7]. The numerical method used to solve the log-conformation evolution equation is explained in detail in Afonso et al [8]. The advective terms were discretized with the CUBISTA high-resolution scheme [9], formally of third-order accuracy. In this work we will focus on creeping-flow conditions, in which case the advective term in the momentum equation is neglected.

Results and Discussion

4:1 Contraction flow

The planar abrupt contraction is sketched in Figure 1. Due to the geometrical simplicity and known numerical difficulties, the planar 4:1 sudden contraction was established as a benchmark flow problem in 1987 [6].

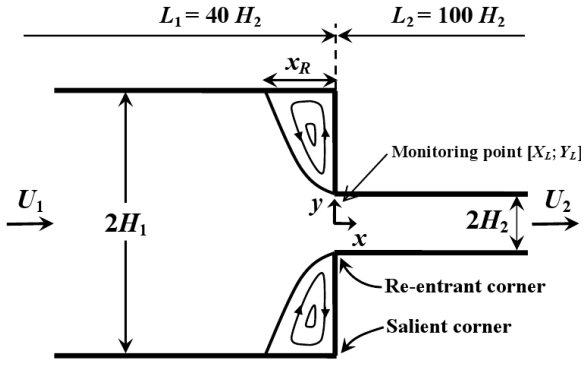

Figure 1. Schematic representation of the 4:1 planar contraction geometry.

All steady and unsteady calculations were obtained with the same time step increment (δt), β=1/9 and were carried out at zero Reynolds number, $Re=\rho U_2 H_2/\eta_0=0$ (creeping flow), where H_2 and U_2 represent the half-width of the downstream channel and the corresponding average velocity. An inlet length $L_1=40H_2$ and an outlet length $L_2=100H_2$ were used to ensure complete flow development upstream and downstream of the contraction (Figure 1). At the inlet the velocity and stress profiles are prescribed by the analytical solutions, whereas at the outlets Neumann boundary conditions are imposed for all computed variables, except pressure which is linearly extrapolated from the two adjacent upstream cells. The Weissenberg number is here defined as $Wi=\lambda U_2/H_2$. Calculations were carried out with a mesh, that maps the whole physical domain, presenting higher concentration of cells near the corner of the contraction and the walls (in such a way that $(\Delta x/H_2)_{min}=(\Delta y/H_2)_{min}=0.0071$).

The results obtained for the time-average corner vortex length ($X_R=x_R/H_2$), are presented in Figure 2. A non-monotonic evolution is observed, with a minimum value of X_R attained at $Wi\approx4.5$ and then more than doubling at Wi=20 relative to the Newtonian value. A similar non-monotonic behaviour was reported by Howell [10], using a continuation algorithm for the discontinuous Galerkin finite element method. The error bars in Figure 2 indicate the amplitude of the X_R oscillations.

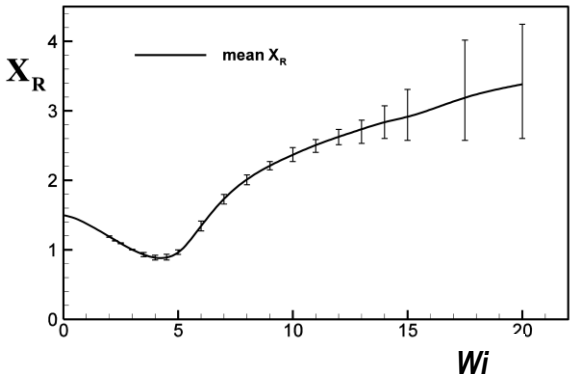

Figure 2.Time average dimensionless length ot primary vortex as function of Wi.

The use of the log-conformation allowed the computations up to Wi=100, approximately one order of magnitude higher than the obtained with the standard version. Also, a new and rich sequence of flow dynamic regimes obtained at high Wi numbers was mapped. At high Wi, a growth of the flow unsteadiness results in asymmetric flow with alternate back-shedding of vorticity from pulsating upstream recirculating eddies. Additionally, a frequency doubling mechanism is also observed, which eventually leads to a chaotic regime at higher Wi. At

sufficiently high Weissenberg numbers, this process becomes more dramatic, in which the size of the main vortices varies substantially and very rapidly, a process accompanied by the formation of upstream secondary vortices, which are shed in the upstream flow direction (Figure 3a-c).

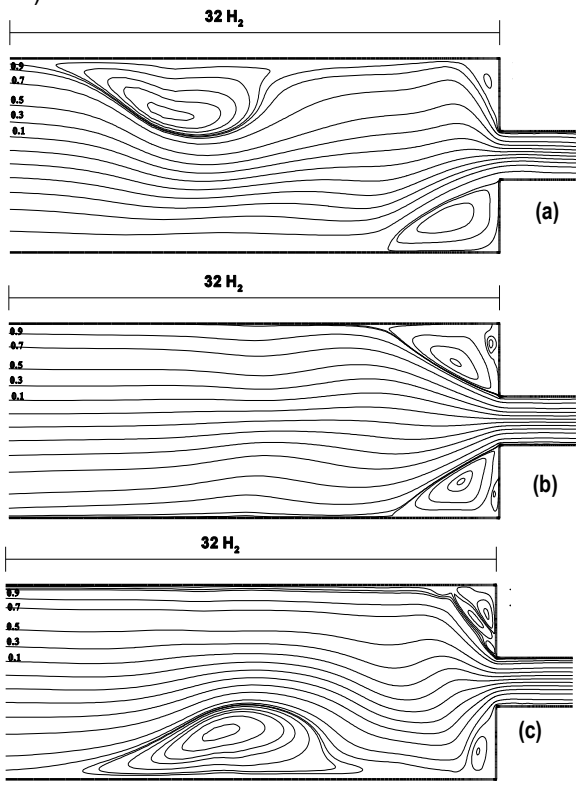

Figure 3. Flow patterns for Wi=100 at different instants.

Cylinder flow

From a numerical point of view, the cylinder flow is considered a smooth flow, due to the absence of geometrical singularities. However, it also introduces some difficulties associated with the development of thin stress layers on the cylinder sidewall and especially along the centreline in the cylinder rear wake. For all these reasons this flow was selected as a benchmark problem in computational rheology [5]. Another reason for the success of this choice was the suitability of this benchmark flow to experimental investigations, especially for birefringence studies.

The geometry of the viscoelastic fluid flow past a confined cylinder in a channel is shown in Figure 4. The ratio of channel half-height h to cylinder radius R is set equal to 2, which corresponds to the 50% blockage case [5].

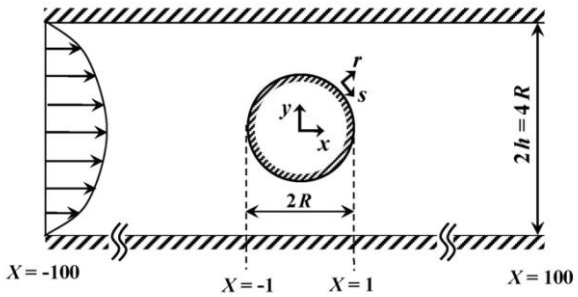

Figure 4. Schematic representation of the cylinder geometry.

The computational domain is 200R long, with 99R upstream and 99R downstream of the forward and rear stagnation points of the cylinder, respectively. The downstream length is sufficient for the flow to become fully-developed and to avoid any effect of the Neumann outflow boundary condition upon the flow in the vicinity of the cylinder. Vanishing axial gradients are applied to all variables, including the pressure gradient, at the outlet plane. No-slip conditions are imposed at both the cylinder surface ($r = R$: $u = 0$, $v = 0$) and the channel wall ($y = \pm h$: $u = 0$, $v = 0$). The mesh used has 45120 computational cells and the minimum normalized cell spacing along the radial and azimuthal directions is 0.004 and 0.0006, respectively. Here again, the calculations were carried out at a vanishing Reynolds number and $\beta = 0.59$. The Weissenberg number is defined as $Wi = \lambda U/R$, where U and R represent average velocity and the cylinder radius, respectively.

The obtained predictions for the dimensionless drag coefficient (K) are presented in Figure 5. Up to $Wi = 1$ the results agree and follow the trend of available data [8,11], presenting a non-monotonic evolution with Wi and a minimum value attained at $Wi \approx 1.4$. Converged simulations were obtained up to $Wi = 200$, which is approximately two orders of magnitude higher than the limit achieved when using the classical extra-stress formulation. At those high Wi a new and rich

sequence of flow dynamic regimes is observed, showing the relevance of the front and rear stagnation points on the cylinder flow.

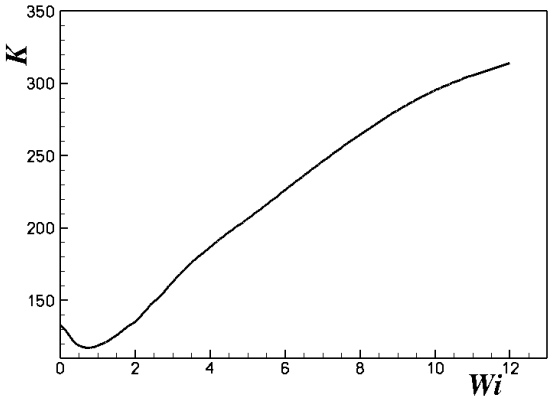

Figure 5.Time average dimensionless drag coefficient as function of Wi.

In addition, the flow at moderate elasticity ($Wi = 10$) is characterized by new elastic induced flow features, such as flow inversion near the cylinder walls due to elastic recoil, as observed in Figure 6a, and at higher Wi ($Wi = 20$) the formation of separated flow regions at the cylinder walls and at the channel walls downstream of the cylinder (Figure 6b).

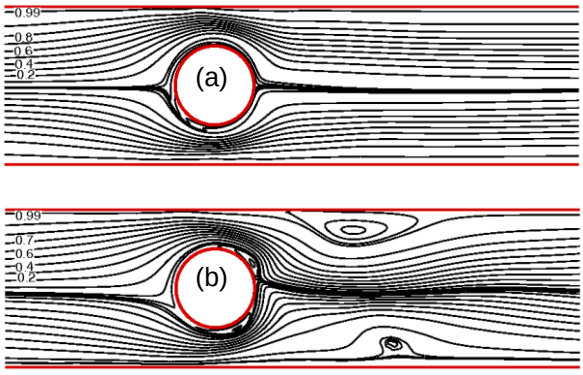

Figure 6. Flow patterns for (a) Wi = 10 and (b) Wi = 20.

Conclusions

For both benchmark flows, converged simulations were obtained up to Wi numbers at least one order of magnitude higher than those obtained with the standard extra-stress formulation: up to $Wi = 100$ on the 4:1 contraction flow and $Wi = 200$ in the confined cylinder flow. Also, new and rich sequences of flow dynamic regimes obtained at high Wi were mapped for both benchmark flows.

Acknowledgements

The authors acknowledge funding from FEDER and Fundação para a Ciência e a Tecnologia (FCT), Portugal, through projects PTDC/EQU-FTT/70727/2006 and PTDC/EQU-FTT/113811/2009. A.M. Afonso would also like to thank FCT for financial support through the scholarship SFRH/BPD/75436/2010.

References

1. R.G. Owens and T.N. Phillips. Imperial College Press, London, (2002);
2. R. Fattal and R. Kupferman, J. Non-Newtonian Fluid Mech., 123, 281–285 (2004);
3. N. Balci, B. Thomases, M. Renardy, C.R. Doering, J. Non-Newtonian Fluid Mech.,166,546-553(2011);
4. A.M. Afonso, F.T. Pinho and M.A. Alves, J. Non-Newtonian Fluid Mech., submitted, (2011);
5. R.A. Brown and G.H. McKinley, J. Non-Newtonian Fluid Mech., 52 (3):407–413, (1994);
6. O. Hassager, J. Non-Newtonian Fluid Mech., 29, 2–5, (1988);
7. P.J. Oliveira, F.T. Pinho, and G.A. Pinto, J. Non-Newtonian Fluid Mech. 79 1–43 (1998);
8. A. Afonso, P.J. Oliveira., F.T. Pinho and M.A. Alves, J. Non-Newtonian Fluid Mech., 157, 55-65 (2009);
9. M.A. Alves, P.J. Oliveira, F.T. Pinho, Int. J. Num. Meth. Fluids, 41, 47–75 (2003).
10. J. S. Howell, J. Comp. Applied Math., 225(1):187–201, (2009).
11. M. A. Alves, F. T. Pinho, and P. J. Oliveira. J. Non-Newtonian Fluid Mech., 97(2-3):207–232, (2001).

Contact Address:

A.M. Afonso (aafonso@fe.up.pt)
Centro de Estudos de Fenómenos de Transporte, Departamento de Engenharia Química, Faculdade de Engenharia da Universidade do Porto, Rua Dr. Roberto Frias s/n, 4200-465, Porto, Portugal.
Telf.:+351 225081400